frontiers | Frontiers in Marine Science

TYPE Original Research
PUBLISHED 31 January 2023
DOI 10.3389/fmars.2023.1038192

Check for updates

OPEN ACCESS

EDITED BY
Daniela Zeppili,
Institut Français de Recherche pour l'Exploitation de la Mer (IFREMER), France

REVIEWED BY
David Emerson,
Bigelow Laboratory For Ocean Sciences, United States
Craig Lee Moyer,
Western Washington University, United States

*CORRESPONDENCE
Céline Rommevaux
celine.rommevaux@mio.osupytheas.fr

SPECIALTY SECTION
This article was submitted to Deep-Sea Environments and Ecology, a section of the journal Frontiers in Marine Science

RECEIVED 06 September 2022
ACCEPTED 12 January 2023
PUBLISHED 31 January 2023

CITATION
Astorch-Cardona A, Guerre M, Dolla A, Chavagnac V and Rommevaux C (2023) Spatial comparison and temporal evolution of two marine iron-rich microbial mats from the Lucky Strike Hydrothermal Field, related to environmental variations. *Front. Mar. Sci.* 10:1038192. doi: 10.3389/fmars.2023.1038192

COPYRIGHT
© 2023 Astorch-Cardona, Guerre, Dolla, Chavagnac and Rommevaux. This is an open-access article distributed under the terms of the Creative Commons Attribution License (CC BY). The use, distribution or reproduction in other forums is permitted, provided the original author(s) and the copyright owner(s) are credited and that the original publication in this journal is cited, in accordance with accepted academic practice. No use, distribution or reproduction is permitted which does not comply with these terms.

Spatial comparison and temporal evolution of two marine iron-rich microbial mats from the Lucky Strike Hydrothermal Field, related to environmental variations

Aina Astorch-Cardona[1], Mathilde Guerre[1], Alain Dolla[1], Valérie Chavagnac[2] and Céline Rommevaux[1]*

[1]Aix Marseille Univ, Université de Toulon, CNRS, IRD, MIO, Marseille, France, [2]Géosciences Environnement Toulouse, CNRS UMR 5563 (CNRS/UPS/IRD/CNES), Université de Toulouse, Observatoire Midi-Pyrénées, Toulouse, France

In hydrothermal environments, diffuse fluids emanations provide optimal conditions for the development of iron-rich microbial mats. Here, we present a unique spatial and temporal study of phylogenetic and chemical data from this type of mats and their associated hydrothermal fluids from two sites of the Lucky Strike Hydrothermal Field (EMSO-Azores deep-sea observatory), collected annually from 2016 to 2020. Our metabarcoding analyses reveal a completely different microbial community at each site, linked to the distinctive chemical composition of the diffuse fluids nourishing the mats. Capelinhos site is dominated by microorganisms with metabolisms related to iron, methane, and reduced sulphur compounds, coming from hydrothermal fluids, while North Tour Eiffel site presents higher abundances of microorganisms with metabolisms related to nitrogen, organic and oxidized sulphur compounds, coming from seawater. We present for the first time the yearly evolution of these mats over a five-year period. This analysis reveals similar variations of the microbial communities over time at both sites, indicating a regional Lucky Strike influence on the temporal scale. We also highlight more diversified microbial communities at both sites in 2016, pointing out the occurrence of a geological event that could have affected them during this specific year. Except for this year, our study shows that the communities of iron-rich microbial mats remain stable over time at both sites.

KEYWORDS

iron-rich microbial mats, microbial communities, environmental variations, temporal evolution, EMSO-Azores, Lucky Strike Hydrothermal Field, spatial comparison

Introduction

In the deep seawater mass at hydrothermal fields, hot, reduced and metal-rich fluids mix with cold and oxygenated seawater, creating redox gradients that allow the development of unique ecosystems based on chemolithoautotrophy (Reysenbach and Shock, 2002). At the seafloor, the diffuse fluids, which consist of a mixture of end-member hydrothermal fluid and seawater that percolates through the oceanic crust and the hydrothermal sediment slabs, create an optimal environment for the development of microbial mats. Depending on the chemical composition of these diffuse fluids, various types of microbial mats have been reported (Crépeau et al., 2011; Hager et al., 2017; McAllister et al., 2019).

Within the Lucky Strike Hydrothermal Field (LSHF), located on the Mid-Atlantic Ridge (MAR, N37°17, W32°17), two main types of microbial mats have been described. White filamentous mats, dominated by Gammaproteobacteria and Campylobacterota, implicated in sulphur oxidation (Crépeau et al., 2011), and orange iron-rich microbial mats (Scott et al., 2015) constructed around iron-oxidizing bacteria (Zetaproteobacteria (Emerson et al., 2007)). LSHF is located ~400 km south-west of the Azores archipelago at an active 65-km-long segment of the MAR (Fouquet et al., 1994). Since the deployment of the EMSO-Azores deep-sea observatory in 2010 (Colaco et al., 2011), a continuous geophysical, geochemical and biological survey of the area has been maintained. This has allowed the study of the vent ecosystems' development according to physico-chemical environmental variations (Cuvelier et al., 2009; Cuvelier et al., 2011; Barreyre et al., 2012; Sarrazin et al., 2015; Chavagnac et al., 2018; Rommevaux et al., 2019), along with the sampling of iron-rich microbial mats and their associated black smoker hydrothermal fluids. Such samples, collected yearly between 2016 and 2020 from two different venting sites, Capelinhos and North Tour Eiffel, are the basis of this work.

The first studies of iron-rich microbial mats were conducted on the hydrothermal vents at the summit of Kama'ehuakanaloa Seamount (previously known as Lō'ihi Seamount) (Hawaii) (Moyer et al., 1995; Emerson and Moyer, 2002), but they have also been described around vents near other seamounts, island arc systems (Makita et al., 2016; Hager et al., 2017) or spreading ridge systems (Scott et al., 2015; Vander Roost et al., 2017). These iron-rich mats are structured as loosely aggregated iron-oxyhydroxides of different shapes combined with exopolysaccharides (Chan et al., 2016). Previous studies have shown that a large phylogenetic diversity is present within these mats, with the coexistence of microorganisms involved in the iron, carbon, sulphur and nitrogen biogeochemical cycles (Scott et al., 2015; McAllister et al., 2021). Nevertheless, recent studies suggested that Zetaproteobacteria, autotrophic iron-oxidizing bacteria that use ferrous iron (Fe(II)) as their sole energy source, play a key role as primary producers in their formation and in the coupling of the iron cycle with the other biogeochemical cycles (Laufer et al., 2017; Makita, 2018; McAllister et al., 2021). While several studies have been carried out to describe, characterize and isolate marine iron-oxidizing bacteria (Laufer et al., 2017; McAllister et al., 2019), fewer studies have investigated the whole microbial community of iron-rich mats (Scott et al., 2016; Vander Roost et al., 2017; McAllister et al., 2021) and none has focused on the assessment of the variability of spatial and temporal environmental conditions on their development.

Here, we present a unique spatial and temporal study of phylogenetic and chemical data on iron-rich microbial mats and their associated hydrothermal fluids. We have investigated the phylogenetic diversity present in these mats *via* high-throughput DNA sequencing of the 16S rRNA gene for Bacteria and Archaea, and we have analyzed the chemical composition of end-member hydrothermal fluids nourishing the mats. The results of the present study demonstrate a spatial difference between the microbial communities of the two studied sites, highlighting a higher hydrothermal contribution and dissolved iron (dFe) supply at Capelinhos' mats than at those of North Tour Eiffel. Our results show a possible influence of methanotrophic and ammonia-oxidizing microorganisms on their development and structuring. Finally, the temporal monitoring of these communities suggests a regional LSHF influence on the temporal scale.

Materials and methods

Site description

LSHF hosts between 20 and 30 active sites consisting of high-temperature black smokers and low temperature diffuse venting areas (Barreyre et al., 2012). All historical sites are located around a fossil lava lake apart from Capelinhos, which was discovered later on in 2013 and is located approximately 1.5 km east of the LSHF (Escartin et al., 2015) (Figure 1, Ondréas et al., 2009). Capelinhos site is characterized by ~10 m high candelabra-shape chimneys discharging fluids at temperatures of up to 324°C (Escartin et al., 2015; Chavagnac et al., 2018), set on a polymetallic sulphide mound hosting a network of diffuse vents at its base. Tour Eiffel site consists of a ~18 m high tower-like main edifice, with 4 or 5 chimneys venting black smoker fluids up to 326°C, surrounded by a large network of fissures where diffuse hydrothermal fluids discharge at temperatures of up to 100°C (Sarradin et al., 2009; Rommevaux et al., 2019). Both Capelinhos and Tour Eiffel venting sites display similar morphological features but their main difference resides in the hydrothermal fluid chemical composition, whereby Capelinhos'

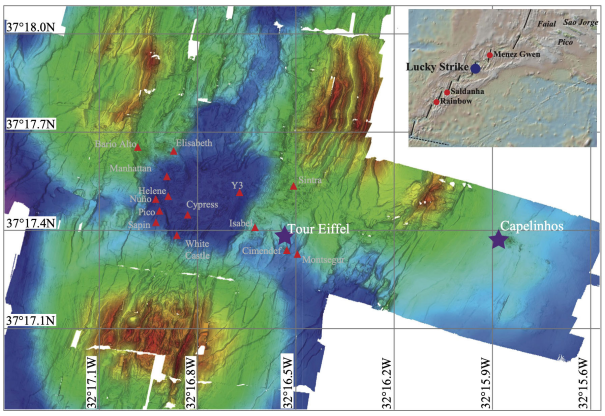

FIGURE 1
Bathymetric map modified from Ondréas et al. (2009), representing the location of the different active sites of the LSHF. Capelinhos and Tour Eiffel sites are marked with a purple star.

fluids contain up to 2800 µM of dFe compared to 574 µM at Tour Eiffel (Chavagnac et al., 2018; Leleu, 2018).

Sample collection

Since 2016 and yearly until 2020, iron-rich microbial mats were collected at Capelinhos and North Tour Eiffel sites during the MoMARSAT EMSO-Azores seafloor observatory maintenance cruises (Cannat and Sarradin (2016), Cannat Mathilde (2018); Sarradin Pierre-Marie, 2017; Sarradin Pierre-Marie, 2019; Sarradin Pierre-Marie, 2020), on board of the R.V. *L'Atalante* and *Pourquoi Pas?* with the Remotely Operated Vehicle (ROV) *Victor 6000* or the Human Operated Vehicle (HOV) *Nautile*. At the seafloor, iron-rich mats covered a surface of about 2500 cm^2 at or in close vicinity of diffuse hydrothermal venting. They were sampled yearly at the same location at both sites, using the grabber of the submersible's hydraulic arm (18 x 16 x 16 cm). Because of sampling size, fine scale structuration of the mats will not be addressed in this study. Samples were placed in previously sterilized bio-boxes to prevent contamination from the surface and from sample flushing during the ascent to the surface. Once onboard, they were transferred under a laminar flow hood, sterilely aliquoted in 5 ml tubes and preserved at -80°C for various on-shore laboratory analyses.

Black smoker hydrothermal fluids were sampled during the 2015 to 2019 MoMARSAT cruises (Sarradin Pierre-Marie, 2015), but not in 2020 due to the Covid-19 pandemic. Black smoker fluids were sampled up to 4 times at Capelinhos and Tour Eiffel chimneys using 200 ml titanium gas-tight syringes with a needle-like snorkel, operated and triggered one by one by the ROV/HOV hydraulic arm. Prior to fluids sampling, the temperature of black smoker hydrothermal fluids was measured *in situ*, using the high-temperature probe of the submersible. Even though diffuse hydrothermal fluids were not sampled, the temperature of these fluids was also measured *in situ* at both sites.

Hydrothermal fluids chemical analyses and data processing

After the ROV/HOV recovery aboard the research vessel, all black smoker hydrothermal fluids were filtered with 0.22-µm Millipore filters and processed as described in Chavagnac et al. (2018). Chemical analyses of hydrothermal fluids were performed at the Géosciences Environnement Toulouse Laboratory (GET, University of Toulouse, France). All details of sample treatment and analytical protocols are presented into details in Besson et al. (2014) and Chavagnac et al. (2018). All solutions were void of any particulate larger than 0.22 µm retained on the filter. As such, iron analyses (dFe) of filtered fluid measured by inductively coupled plasma atomic emission spectrometry (Horiba Jobin Yvon Ultima 2), as described in Chavagnac et al. (2018), mainly represent the soluble Fe(II), given the environmental conditions. Dissolved hydrogen sulphide (dH_2S) concentrations were measured in the solution with an amperometric micro-sensor (AquaMS, France).

Chemical data of black smoker hydrothermal fluids was used to calculate the composition of end-member hydrothermal fluids by linear extrapolation to Mg-zero levels of the least-square regression method (Von Damm, 1988). The calculated end-members are reported in Table 1 and the chemical data of each sample can be found in Table S1 of the Supplementary Information. End-member dFe and dH_2S concentrations were used to assess the influence of environmental parameters in iron-rich mats microbial communities.

In addition, the contribution of end-member hydrothermal fluid to diffuse fluids was quantified based on physical parameters, *i.e.* temperature measured *in situ*, and on adiabatic conservative mixing between end-member hydrothermal fluid and seawater.

DNA extraction

Total genomic DNA was extracted in triplicate from each iron-rich mat sample. Due to the heterogeneity of these type of samples, extracting in triplicate allows to maximize the DNA retrieved from them. As the yield and composition of DNA depend on the DNA extraction protocol used (Alain et al., 2011), two different kits were utilized, to increase the quantity and diversity of obtained DNA and thus the study's accuracy. The FastDNA® SPIN Kit for Soil (MP Biomedicals, Santa Ana, CA, USA) and the DNeasy® PowerSoil® Kit (QIAGEN, Hilden, Germany) were used following the manufacturer's instructions. For both kits, cell lysis was performed using the FastPrep® Instrument (MP Biomedicals, Santa Ana, CA, USA). The extracted DNA was quantified using the QuantiFluor dsDNA System (PROMEGA, Madison, USA) and the Qubit 2.0 Fluorometer (Invitrogen Thermo Fisher Scientific). For each sample, the six extraction products (triplicates from both kits) were pooled together prior to sequencing.

16S rRNA gene sequencing and sequence processing

16S rRNA gene sequencing was performed using the Illumina MiSeq technology (MR DNA, Shallowater, TX, USA) in two different sequencing runs, the first one for the 2016 to 2019 samples and the second one for the 2020 samples. 30 µl aliquots of the pooled DNA for each sample were sent to MR DNA (Shallowater, TX, USA), who performed the PCRs and the library preparation for sequencing. The primers targeting the V3-V4 hypervariable regions of the 16S rRNA gene for Bacteria were 341F (5'-CCTACGGGNGGCWGCAG-3') and 785R (5'-GACTACHVGGGTATCTAATCC-3') (Herlemann et al., 2011) for both runs. The primers targeting the V3-V4 regions for Archaea were A344F (5'-AYGGGGYGCASCAGGSG-3') (Stahl and Amann, 1991) and A806R (5-GGACTACVSGGGTATCTAAT-3') (Takai and Horikoshi, 2000) for the first run and A349F (5'-GYGCASCAGKCGMGAAW-3') (Takai and Horikoshi, 2000) and A806R (5'-GGACTACVSGGGTATCTAAT-3') for the second run.

Data analysis was performed in the R environment (R Core Team (R Foundation for Statistical Computing), 2020) unless otherwise specified. Raw Illumina sequences were demultiplexed using the

TABLE 1 Chemical composition of end-member hydrothermal fluids calculated from the black smoker hydrothermal fluids collected at Capelinhos and Tour Eiffel sites between 2015 and 2019.

Site	Year	Sample name	Mg mmol/l	Ca mmol/l	K mmol/l	Na mmol/l	Fe µmol/l	Mn µmol/l	Si mmol/l	Cl mmol/l	SO_4^{2-} mmol/l	Sr µmol/l	Ba µmol/l	Br µmol/l	Li µmol/l	H_2S mmol/l
CAPELINHOS	**2015**	**end-member**	**0.00**	**17.05**	**12.62**	**214**	**2494**	**594**	**13.00**	**267**	**-0.33**	**35.1**	**18.9**	**415**	**120**	**0.83**
		±		0.12	0.03	0.6	44	12	0.05	0.7	0.09	0.2	5.3	2	70	0.10
	2016	**end-member**	**0.00**	**17.76**	**9.92**	**220**	**2131**	**537**	**14.73**	**288**	**0.61**	**46.1**	**12.6**	**463**	**308**	**1.08**
		±		0.52	0.29	12	242	45	1.21	24	2.29	6.1	3.6	35	33	0.05
	2017	**end-member**	**0.00**	**19.42**	**11.62**	**254**	**2294**	**539**	**12.57**	**277**	**0.05**	**35.9**	**4.3**	**447**	**168**	**0.88**
		±		0.15	0.03	3	50	4	0.12	2	0.25	1.0	0.9	5	4	0.10
	2018	**end-member**	**0.00**	**19.80**	**11.27**	**245**	**2600**	**666**	**12.94**	**268**	**-0.07**	**35.4**	**21.0**	**508**	**138**	**14.53**
		±		0.14	0.07	1	92	24	0.07	5	0.13	0.6	4.9	71	12	3.85
	2019	**end-member**	**0.00**	**24.98**	**13.95**	**238**	**1768**	**492**	**13.12**	**293**	**0.98**	**44.2**	**2.2**	**525**	**177**	**5.99**
		±		0.72	0.24	12	235	29	0.55	16	2.04	2.9	0.5	46	8	0.46
TOUR EIFFEL	**2015**	**end-member**	**0.00**	**35.85**	**20.96**	**341**	**584**	**269**	**14.24**	**428**	**0.08**	**74.1**	**8.2**	**680**	**335**	**0.97**
		±		0.06	0.005	0.4	18	7	0.05	0.4	0.16	0.5	4.2	5	2	0.06
	2016	**end-member**	**0.00**	**35.06**	**16.84**	**331**	**382**	**190**	**15.20**	**443**	**-0.03**	**73.6**	**14.2**	**689**	**442**	**0.85**
		±		0.40	0.14	3	10	5	0.39	4	0.01	3.1	0.7	5	17	0.17
	2017	**end-member**	**0.00**	**37.50**	**19.25**	**369**	**599**	**269**	**15.37**	**427**	**0.10**	**77.3**	**18.9**	**645**	**481**	
		±		0.10	0.08	2	17	7	0.28	1	0.17	1.8	4.8	26	19	
	2018	**end-member**	**0.00**	**39.08**	**18.67**	**336**	**478**	**234**	**14.55**	**398**	**1.47**	**66.1**	**10.7**	**635**	**294**	**0.70**
		±		0.47	0.13	1	19	4	0.42	17	0.46	1.1	4.0	29	6	0.03
	2019	**end-member**	**0.00**	**42.66**	**22.33**	**345**	**391**	**159**	**13.95**	**433**	**0.01**	**71.2**	**12.0**	**725**	**266**	**10.51**
		±		1.29	0.48	8	12	4	0.41	0.4	0.02	0.7	0.9	11	4	0.55

Chemical composition of black smoker samples can be found on Table S1 of the Supplementary Information.
The values in bold represent the element concentrations in the end-member hydrothermal fluids while the values that are not in bold are the standard deviations.

FASTQ processor free software (MR DNA, Shallowater, TX, USA). Bacterial and archaeal sequences were treated separately with the DADA2 pipeline (Callahan et al., 2016), which includes the full amplicon workflow. Reads from each run were treated independently until the chimera identification step. Reads were filtered by quality, sequences shorter than 150bp were removed and maximum expected error was set at 3 for both forward and reverse reads. Based on the quality profiles, trimming parameters were set as follows: trimLeft=0 for both bacterial and archaeal sequences and trimRight=30 or 40 depending on the run. Subsequent steps of the pipeline were carried out using default parameters. The chimera detection and removal step was performed using default parameters on the unique Amplicon Sequence Variant (ASV) table, combining the ASV tables obtained for each run.

All the following analyses were done separately for bacterial and archaeal communities.

Phylogenetic analyses

A taxonomic assignment of the obtained ASVs was performed using the SILVA 138.1 database (Quast et al., 2013). The ASV sequence table was merged with the phylogeny and the metadata of the samples with the phyloseq package (McMurdie and Holmes, 2013). ASVs corresponding to kingdoms other than Bacteria or Archaea were eliminated from the bacterial or archaeal dataset respectively. To be able to compare among the different samples, a rarefaction step was performed, which consisted in subsampling the ASV tables to the lowest sequencing-depth to obtain the same amount of reads for all samples.

To represent the taxonomic composition of the microbial communities by site, heat trees from the metacoder package (Foster et al., 2017) were constructed, summing the abundances of each ASV from each year at each site. Only the 100 most abundant ASVs were

considered to generate these graphics, reads for each taxon can be found in Tables S5 and S6 of the Supplementary Information.

The temporal evolution of the phylogenetic diversity was represented as a bar plot by aggregating the taxa at the phylum level. For the Proteobacteria phylum, the taxa were also aggregated at the class level. Within this paper we have chosen to keep the Proteobacteria phylum nomenclature, in agreement with the SILVA 138.1 database, even though it has been recently renamed Pseudomonadota (Oren and Garrity, 2021).

We used the Basic Local Alignment Search Tool (Altschul et al., 1990) to calculate sequence similarity of the most representative and abundant ASVs sequences of our dataset. This step was performed to refine the taxonomic assignment to the species level if possible. All the microorganisms cited in the results section were identified with more than 96% sequence identity.

Alpha and beta diversity analyses

The phyloseq package was used to analyse the rarefaction curves and assess the quality of the sequencing, and to calculate the alpha and beta diversity indices of the samples, while the ggplot2 package (Wickham, 2016) was used to plot the results.

The Shannon diversity index was calculated to represent the alpha diversity. For comparing the alpha diversity between sites, we used the average illustrated in a boxplot at each site. A Non-Metric Multidimensional Scaling (NMDS) analysis was performed to represent the beta diversity, allowing the visualization of similarities and differences among the microbial communities either between sites or between years at each site. The ordinations were produced using distance matrices calculated according to the Bray-Curtis dissimilarity index, as the number of null values between samples does not affect it. A Permutational Multivariate Analysis of Variance (PERMANOVA, from the vegan package (Oksanen et al., 2020)) using distance matrices was performed only to assess whether the differences observed in the NMDS between sites were significant, with 5 samples in each site considered as replicates. The threshold of significance was set at a p-value of 0.05.

Influence of environmental parameters

To assess the potential effect of selected environmental parameters on the observed differences in the microbial communities' composition, a distance-based Redundancy Analysis (db-RDA, from the vegan package) was performed, using the Bray-Curtis dissimilarity index and standardized data from 2016 to 2019, as environmental data for 2020 was not available. These analyses were performed using dFe and dH_2S concentrations from the end-member hydrothermal fluids as environmental parameters. dFe concentration was selected for this analysis due to the nature of the microbial communities studied, strongly influenced by iron. Because these communities develop within a hydrothermal context, another important environmental parameter was sulphur, represented in our study by dH_2S. An ANOVA like permutation test for db-RDA (from the vegan package) was performed to assess the significance of dFe and dH_2S influence on the microbial communities, as our variables did not follow a normal distribution.

Quantitative PCR

Quantitative PCR (qPCR) was performed on the same DNA pools that were sent for sequencing. Performing qPCR allows to have a more direct comparison of bacterial and archaeal relative abundance in the samples, as sequencing was performed using separate primer sets targeting 16S rRNA genes. qPCR was performed on a CFX96 Real-Time PCR System (Bio-Rad, California, USA) with the primers DGGE300F (5′-GCCTACGGGAGGCAGCAG-3′) (Muyzer et al., 1993) and Univ516 (5′-GTDTTACCGCGGCKGCTGRCA-3′) (Takai and Horikoshi, 2000) for Bacteria and Arc931F (5′-AGGAATTGGCGGGGGAGCA-3′) (Jackson et al., 2001) and m1100R (5′-BTGGGTCTCGCTCGTTRCC-3′) (Einen et al., 2008) for Archaea. Each qPCR reaction mixture contained 5 µl of SYBR® Green Master Mix (Bio-Rad, California, USA), primers at 0.5 µM, DNAse-free water and 2 µl of DNA in a final volume of 10 µl. Each reaction was performed in triplicate and each plate also contained a standard curve and a negative control sample. The standard curves were obtained by serially diluting (10^{-4} to 10^{-8}) plasmids harboring 16S rRNA gene fragments specific for Bacteria or Archaea. The PCR program for Bacteria consisted of a 2 minutes initial denaturation step at 98°C, followed by 30 successive cycles of a 5 seconds denaturation step at 98°C, an hybridization step of 10 seconds at 55°C and a 12 seconds elongation step at 72°C. Finally, a 10 seconds denaturation step at 95°C was performed. The PCR program for Archaea consisted of a 3 minutes initial denaturation step at 98°C, followed by 35 successive cycles of a 10 seconds denaturation step at 98°C, a hybridization step of 10 seconds at 62°C and a 20 seconds elongation step at 72°C. Finally, a 10 seconds denaturation step at 95°C was performed. Melting curves were generated at the end of each qPCR from 65 to 95°C (in 0.5°C steps) for both Bacteria and Archaea. To obtain the relative abundance of bacterial and archaeal communities within the samples, the percentage of each kingdom was calculated out of the sum of Bacteria and Archaea 16S rRNA gene copies in each pool.

Results and discussion

Sites with distinctive chemical signatures over time

The understanding of hydrothermal circulation at LSHF has drastically changed since the discovery of Capelinhos site in 2013, which is located 1.5 km east of previously discovered sites (Escartin et al., 2015) (Figure 1). Even though a unique hydrothermal fluid is feeding the whole LSHF, Capelinhos dFe concentrations (2789.4 ± 84.8 µM) are 4 to 15 times higher than those of historical sites from LSHF (ranging from 185.5 to 686.7 ± 11.3 µM) (Chavagnac et al., 2018). These distinctive chemical characteristics reflect the rapid discharge of hydrothermal fluid from the reaction zone at Capelinhos *via* a fracture zone. The chemical composition of

Capelinhos' end-member hydrothermal fluid has remained essentially similar since 2013, and for the 2015 to 2019 period as presented here (Table 1). This supports the fundamental role of high angle fracture zone as a main conduit to discharge end-member hydrothermal fluid from the reaction zone to the seafloor and limiting subsequent interaction with the surrounding rocks along the upflow zone. Regarding Tour Eiffel site, located at the south-east side of the fossil lava lake (Figure 1), the end-member hydrothermal fluids show consistently over the 2015 to 2019 time-period lower dFe concentrations (ranging from 382 to 599 µM) by a factor of 4 to 7 than those of Capelinhos (ranging from 1768 to 2600 µM) (Table 1). These chemical features indicate the effect of conductive cooling induced by the permeability gradient along the upflow zone, leading to ~65% loss of dFe at depth (Chavagnac et al., 2018). Consequently, diffuse fluids, which are a mixture of end-member hydrothermal fluid and seawater, contain distinctive dFe concentrations at the two sites for similar hydrothermal contribution, *i.e.* Capelinhos diffuse fluids would contain 4 to 7 times more dFe than those at North Tour Eiffel. As a result, microbial mats nourished by diffuse venting should adapt to these differing environmental conditions.

Site effect on the diversity of iron-rich microbial mats' communities

qPCR analyses showed that at both sites, iron-rich microbial mats were largely dominated by Bacteria (90.8 – 99.5%) and had a very small proportion of Archaea (0.5 - 9.2% (Table S2 of the Supplementary Information)), which is in agreement with previous studies (Vander Roost et al., 2017).

The microbial diversity of each site was determined *via* 16S rRNA gene metabarcoding analysis. The percentage of retained 16S rRNA gene sequencing reads after treatment with the DADA2 pipeline and the taxonomic affiliation varied between 41% and 75% for Bacteria and between 22% and 69% for Archaea (Table S3 of the Supplementary Information). The rarefaction curves obtained reached a plateau in almost all samples, except for the 2016 bacterial and archaeal sequencing from North Tour Eiffel, and for the 2019 bacterial sequencing of the same site (Figure S1 of the Supplementary Information). This means that the sequencing effort was strong enough for most of the samples and therefore that the present results are representative.

The Shannon index, representing the alpha diversity, revealed that in average, both the bacterial and the archaeal communities (Figure 2A) were more diversified at North Tour Eiffel than at Capelinhos. Calculations of the Shannon index and other diversity indices can be found in Table S4 of the Supplementary Information. The NMDS plots representing the beta diversity highlighted two distinct clusters depending on the site for bacterial communities (Figure 3A), except for the 2016 sample of North Tour Eiffel, which could be explained by the rarefaction curve not reaching a plateau on this specific sample. The same was observed for archaeal communities (Figure 3B), except in 2020 for both sites. However, one cannot rule out that it could be due to the use of different primer couples for the sequencing of these samples. The PERMANOVA analyses yielded p-values of 0.009 for Bacteria and 0.027 for Archaea, indicating that the differences observed in the NMDS plots between sites were significant. The db-RDA performed on the bacterial and archaeal communities revealed a clear distribution of the samples by site depending on dFe concentration (Figure 4). All Capelinhos samples were positioned along the left side of axis CAP1, while those taken at North Tour Eiffel were located on the right side, indicating that dFe had a higher influence on the microbial communities of Capelinhos than on those of North Tour Eiffel. The influence of dFe was confirmed by the ANOVA like permutation test for db-RDA, which yielded p-values of 0.012 for Bacteria and of 0.03 for Archaea. On the contrary, the same analysis showed that dH_2S did not significantly influence the distribution of the samples. This is in line with

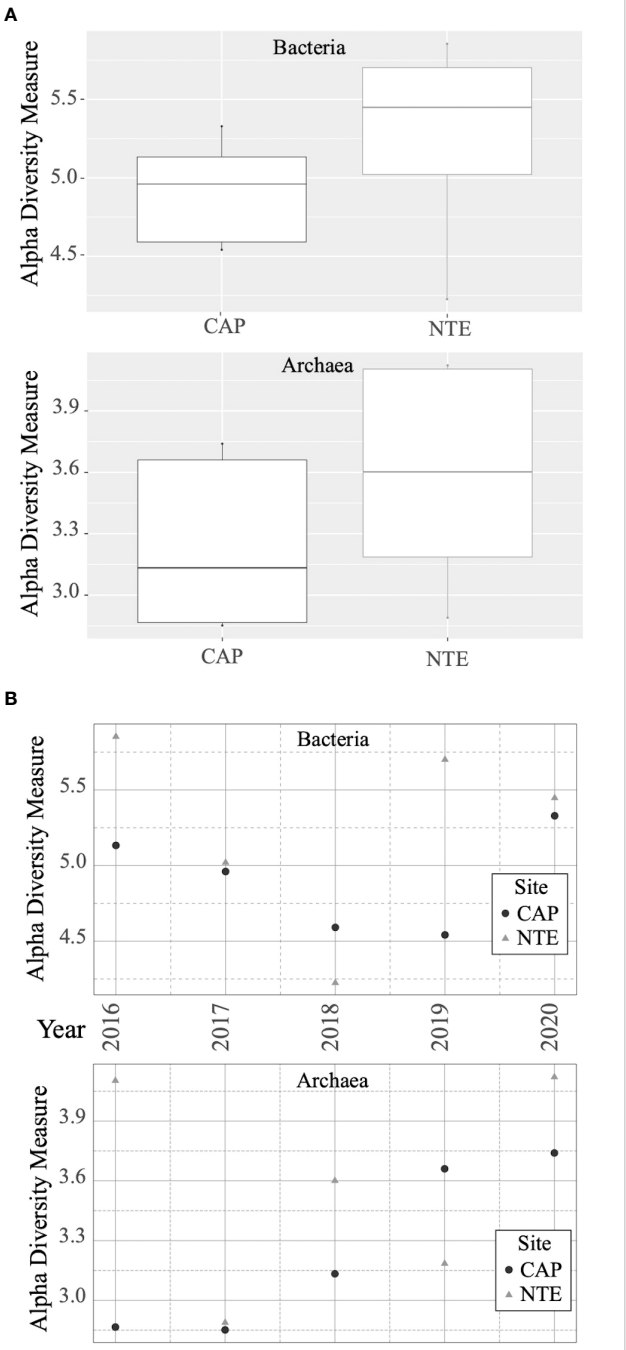

FIGURE 2
(A) Boxplot representing the Shannon diversity index calculated for each site (Capelinhos in black and North Tour Eiffel in gray) for bacterial and archaeal communities. **(B)** Shannon diversity index calculated for each site (Capelinhos in black and North Tour Eiffel in gray) and each year for bacterial and archaeal communities.

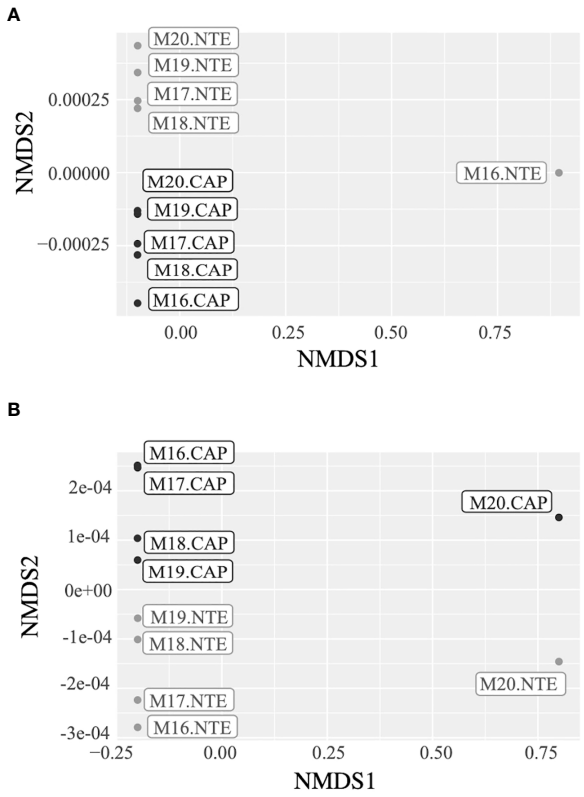

FIGURE 3
NMDS plots representing the differences between **(A)** the bacterial communities' structure and **(B)** the archaeal communities' structure of Capelinhos (black) and North Tour Eiffel (grey) sites.

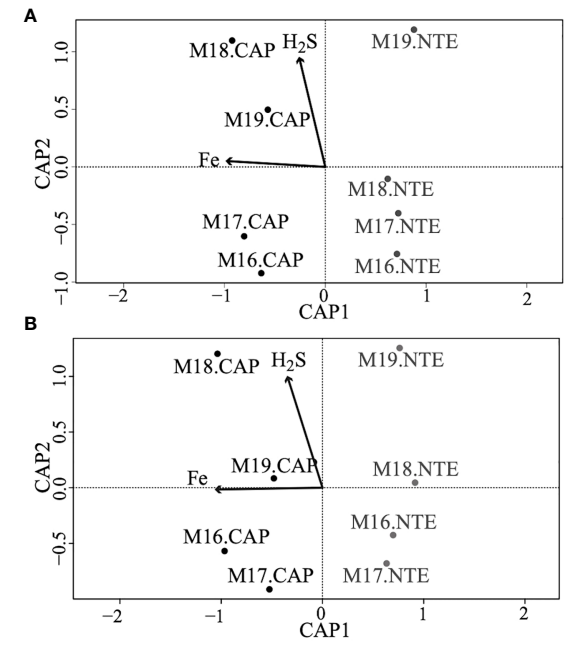

FIGURE 4
db-RDA plots representing the distribution of the samples from Capelinhos (black) and North Tour Eiffel (grey) sites depending on environmental parameters, **(A)** depicting bacterial communities, and **(B)** depicting archaeal communities. Samples from 2020 were not included in these plots as no hydrothermal fluid samples could be collected on that year due to the Covid-19 pandemic.

the higher dFe concentrations of Capelinhos' diffuse fluids compared to those of North Tour Eiffel. The above-mentioned results of the alpha, beta diversity and db-RDA (Figures 2–4), confirm that these environmental differences between sites impact the structure of their microbial communities. These results are consistent with similar comparisons of other iron-rich microbial mats at the Mariana region and at the Arctic Mid-Ocean Ridge (Hager et al., 2017; Vander Roost et al., 2017).

Environmental-related trends on the taxonomic composition of each microbial community

The heat trees representing the bacterial and archaeal 100 most abundant ASVs of Capelinhos and North Tour Eiffel sites (Figure 5) revealed in more details the differences in the microbial composition at each site. The percentages given in the following paragraphs represent the percentages of each taxon out of total reads for each type of community (Tables S5 and S6 of the Supplementary Information).

The bacterial communities were dominated at both sites by Proteobacteria (51.4% at Capelinhos and 48.7% at North Tour Eiffel), followed by Bacteroidota (13% at Capelinhos and 11.4% at North Tour Eiffel) and Patescibacteria (11.3% at Capelinhos and 7.4% at North Tour Eiffel). The archaeal communities were dominated by Nanoarchaeota (51%) at Capelinhos while at North Tour Eiffel they were dominated by Crenarchaeota (41%). Halobacterota was very abundant and more diversified at Capelinhos (29.5%) than at North Tour Eiffel (11.4%).

Within Proteobacteria, Zetaproteobacteria, represented by the *Mariprofundus* genus (Emerson et al., 2007), were always present in the microbial mats' communities at both sites, with a higher abundance at Capelinhos (14.5%) than at North Tour Eiffel (10.8%). As previously described, Zetaproteobacteria are considered primary producers in these mats (McAllister et al., 2021), as autotrophic bacteria using dissolved Fe(II) as their sole energy source, which originates essentially from hydrothermal fluids (Emerson et al., 2007; Makita, 2018; McAllister et al., 2019). As described in Chavagnac et al. (2018) and as shown in Table 1, dFe concentration was higher at Capelinhos, explaining the higher abundance of Zetaproteobacteria at this site. Zetaproteobacteria are known for forming Fe(III)-oxyhydroxides associated with exopolysaccharides (Chan et al., 2011; Bennett et al., 2014) that can potentially be used by other microorganisms to grow, such as iron-reducers or organotrophs (McAllister et al., 2021). This could explain the high abundance of Bacteroidota, represented by heterotrophic bacteria (Allen et al., 2006; Bauer et al., 2016; Iino et al., 2010), and Patescibacteria, extremely small, symbiotic cells with limited metabolic capacities (Castelle et al., 2017; Sieber et al., 2019). Moreover, at Capelinhos some abundant ASVs were related with *Geoglobus ahangari*, *Thermococcus indicus* and *Aciduliprofundum boonei*, three Fe(III)-reducing archaea (Kashefi et al., 2002; Reysenbach et al., 2006; Lim et al., 2020). At North Tour Eiffel, some other bacterial ASVs were also related to Fe(III) reduction, particularly to *Geopsychrobacter electrodiphilus*, a bacterium which can couple the reduction of Fe(III) to the oxidation of organic compounds (Holmes et al., 2004). Essentially, the microbial communities analysis was consistent with an active microbial iron

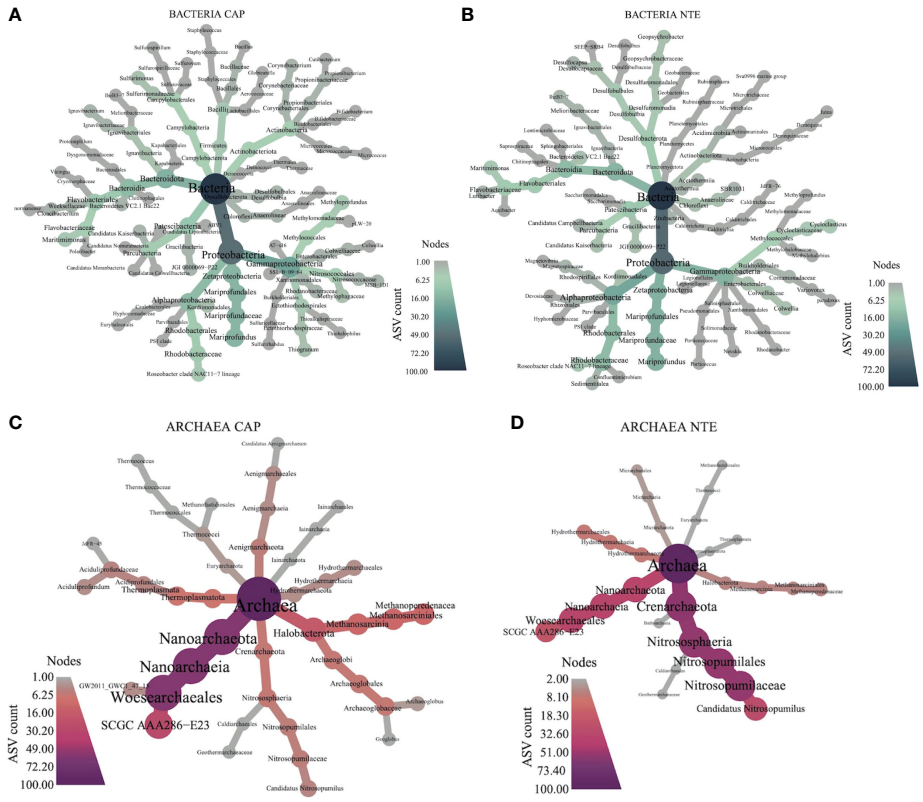

FIGURE 5
Heat trees depicting the sum of bacterial ASVs counts per-taxon of **(A)** Capelinhos and **(B)** North Tour Eiffel, and the sum of archaeal ASVs counts per-taxon of **(C)** Capelinhos and **(D)** North Tour Eiffel. The size and color of the nodes of each cladogram show the number of taxa identified at that taxonomic level.

cycle within these mats, with the co-existence of both iron oxidizers and reducers.

Overall, our results showed that the microbial communities at Capelinhos were dominated by microorganisms with metabolisms related to iron, methane, and reduced sulphur compounds. The most abundant bacterial ASV at Capelinhos was related to *Methyloprofundus sedimenti*, an obligate methane-oxidizing Gammaproteobacteria (Tavormina et al., 2015), revealing the importance of methane on the structuring of these mats. Indeed, Quaiser et al. (2014) revealed by metatranscriptomic analyses that iron and methane oxidation occur simultaneously in freshwater iron-rich microbial mats and that both groups of microorganisms play critical roles in their functioning. Other methanotrophic and methylotrophic microorganisms were also highly abundant within the archaeal communities, such as members of the *Candidatus_Methanoperedens* genus (Halobacterota). Different studies have suggested that members of this genus could potentially couple anaerobic methane oxidation with Fe(III), manganese or nitrate reduction (Haroon et al., 2013; Cai et al., 2018; Leu et al., 2020). The potential use of Fe(III) by some of them could corroborate the primary producers' role of Zetaproteobacteria as Fe(III) suppliers. Nevertheless, the relative abundance of Archaea was much lower (between 0.5% and 8.6% at Capelinhos, Table S2 of the Supplementary Information) than that of Bacteria within these mats, and therefore further microbial interaction analyses would be needed to confirm this correlation in anoxic conditions. On the other hand, very few ASVs related with methanogenic microorganisms were found within the mats, indicating that the methane present in the fluids in which they thrive is likely derived from the diffuse fluids. In agreement, previous studies have shown that LSHF hydrothermal fluids contain a high concentration of methane (Charlou et al., 2000; Rommevaux et al., 2019), which could sustain the presence of methanotrophic microorganisms. Furthermore, quite abundant bacterial ASVs were related to *Sulfurimonas sediminis* (Campylobacterota), an hydrogen- and sulphur-oxidizing bacterium (Wang et al., 2021) or to *Thiogranum longum* (Gammaproteobacteria), a bacterium growing by oxidizing inorganic sulphur compounds (Mori et al., 2015). Some archaeal ASVs were related to *Aciduliprofundum boonei* (Thermoplasmatota), which can reduce elemental sulphur (Reysenbach et al., 2006). The high abundance of autotrophic microorganisms utilizing iron, methane and reduced sulphur compounds, which have been largely described on hydrothermal environments, revealed that diffuse fluids play a key role on the development of Capelinhos mats. Our results also showed a high abundance of members of the *Archaeoglobaceae* family (Halobacterota). Some ASVs were related to *Archaeoglobus veneficus*, a facultative autotrophic sulphite or thiosulphate reducer (Huber et al., 1997) or to *Archaeoglobus sulfaticallidus*, a facultative autotrophic sulphate-reducer (Steinsbu et al., 2010). These microorganisms, substantially described on hydrothermal environments, could be sustained by the sulphate coming from the seawater and diffuse fluids mixture. Within the mats, an important diversity of organotrophic microorganisms were also highly present. Among

these organotrophic microorganisms, members of the *Roseobacter* clade (Alphaproteobacteria), described as an ubiquitous marine group (Luo and Moran, 2014), were quite abundant. The presence of other organotrophic bacteria like members of the Gracilibacteria class (Patescibacteria) or the *Maritimimonas* genus (Bacteroidota), confirms that the autotrophic primary producers of these mats recruit other microorganisms coming mainly from the diffuse fluids but also from seawater, to construct iron-rich microbial mats.

At North Tour Eiffel, the microbial mats were also composed of microorganisms with metabolisms related to iron, methane, or reduced sulphur compounds but with a lower incidence than at Capelinhos. At this site, the microbial communities were dominated by microorganisms with metabolisms related to organic compounds, nitrogen, and oxidized sulphur compounds. The most abundant bacterial ASVs at this site were mostly related to organotrophic microorganisms retrieved from seawater or from sea-tidal sediments. Among them, there were members of the *Rhodobacteraceae* family (Alphaproteobacteria) (Swingley et al., 2007; Xu et al., 2021; Ding et al., 2020; Jeong et al., 2015), the *Maritimimonas* (Bacteroidota) (Park et al., 2009), *Variovorax* (Satola et al., 2013) and *Cycloclasticus* (Staley, 2010) genus (Gammaproteobacteria), or the Patescibacteria, Planctomycetota (Kallscheuer et al., 2020) and Zixibacteria phyla. The archaeal community was dominated by members of the Crenarchaeota, closely related to *Nitrosopumilus oxyclinae* (Qin et al., 2017), *Nitrosopumilus zosterae* (Nakagawa et al., 2021) and *Nitrosopumilus adriaticus* (Bayer et al., 2019), all identified as marine ammonia-oxidizing archaea. The co-existence of Zetaproteobacteria and *Nitrosopumilus* has already been reported by Vander Roost et al. (2017), who proposed that members of this genus could assist in the formation of iron mats, creating a link between iron and nitrogen metabolisms. The dominance of this archaeal phylum, together with the high abundance of organotrophic bacterial ASVs coming as well from seawater, confirms that seawater and its organic compounds play an important role in the structure and composition of the mats developing at North Tour Eiffel. Oxidized sulphur compounds also played a key role in structuring these communities, with a number of the most abundant bacterial ASVs identified as belonging to either *Desulfocapsa* genus (Desulfobacterota), whose cultured bacteria are known to reduce sulphate or disproportionate inorganic sulphur compounds (Finster et al., 2013), or to *Desulfomarina profundi* (Desulfobacterota), a chemolithoautotrophic sulphate-reducing bacterium (Hashimoto et al., 2021). The presence of oxidized sulphur compounds in the diffuse fluids at North Tour Eiffel is corroborated by the longer residence time of hydrothermal fluids along the upflow zone to the seafloor at this site, which implies that reduced sulphur compounds could be altered by conductive cooling.

Influence of hydrothermalism on the development of iron-rich microbial mats

In this study, we do not have samples of the diffuse fluids nourishing the mats from their base, but end-member hydrothermal fluid data showed that Capelinhos' fluids have a higher concentration of dFe and dH_2S than those from North Tour Eiffel (Table 1). In addition, the calculation of the contribution of end-member hydrothermal fluids in diffuse fluids using temperature measured *in situ* showed that, in general, this contribution was higher at Capelinhos (32%) than at North Tour Eiffel (12 to 17%), suggesting that Capelinhos diffuse fluids would have higher dFe and dH_2S concentrations than those of North Tour Eiffel, favoring the development of microorganisms related to them. Moreover, the seawater above the mats is also impacted by current- and tidal-related fluxes, which varies in time and space (Barreyre et al., 2014). Indeed, our results revealed that the microbial community of Capelinhos was dominated by microorganisms thriving in hydrothermal fluids, while that of North Tour Eiffel had higher abundances of microorganisms related to seawater. These results showed, as different studies have already suggested, that the variability in energy density of the fluids surrounding the mats, shape their microbial communities' composition (Dahle et al., 2015; Vander Roost et al., 2017). Besides, little is known about microorganisms' interactions at iron-rich microbial mats. Here, we report the co-existence of iron-oxidizing microorganisms with both methanotrophic and ammonia-oxidizing microorganisms, which confirms the need of more in-depth studies of these relationships and of key environmental parameters to better constrain the functioning of Zetaproteobacteria themselves.

Temporal evolution of iron-rich microbial mats over five years

Here, we present for the first time an analysis of the microbial composition variations of two different iron-rich mats during five consecutive years.

The bar plot graph revealed in more details the variations over time of the different microbial communities' abundances at the phylum level in each sampling site (Figure 6A for Bacteria and 6B for Archaea). Reads for each taxon can be found in Tables S5 and S6 of the Supplementary Information. Only phyla with more than 1% of abundance were considered here. We have reported two representative environmental parameters (dFe and dH_2S) on this graph (Figure 6, see data on Table 1) as line plots superposed to the bar plots in order to show environmental variations through time. We observed a variation of Proteobacteria phylum, which remained dominant over time at both sites, in accordance with previous studies performed on other iron-rich microbial mats (Quaiser et al., 2014; Vander Roost et al., 2017). At Capelinhos, the abundance of Proteobacteria was at its lowest in 2016 (31.8%), fluctuated in 2017, 2018 and 2019 (around 47 - 55%) and reached its maximal occurrence in 2020 (70.2%). At North Tour Eiffel, their abundance fluctuated in 2016, 2017, 2019 and 2020 (around 38 - 49%), and presented higher occurrences in 2018 (64.6%).

Zetaproteobacteria class showed high incidences in all the samples but with variations in abundance that were correlated with variations in the dFe concentration of the end-member hydrothermal fluids. At Capelinhos, Zetaproteobacteria were dominant in 2018 and 2019 (23.7% and 20.2%, respectively), and their abundance was lower in 2016, 2017 and 2020 (around 4.2 - 17.3%). At North Tour Eiffel, they did not dominate the bacterial community in any year, but always had a quite elevated abundance (around 6 - 13.3%). As previously mentioned, the amount of available dFe in the

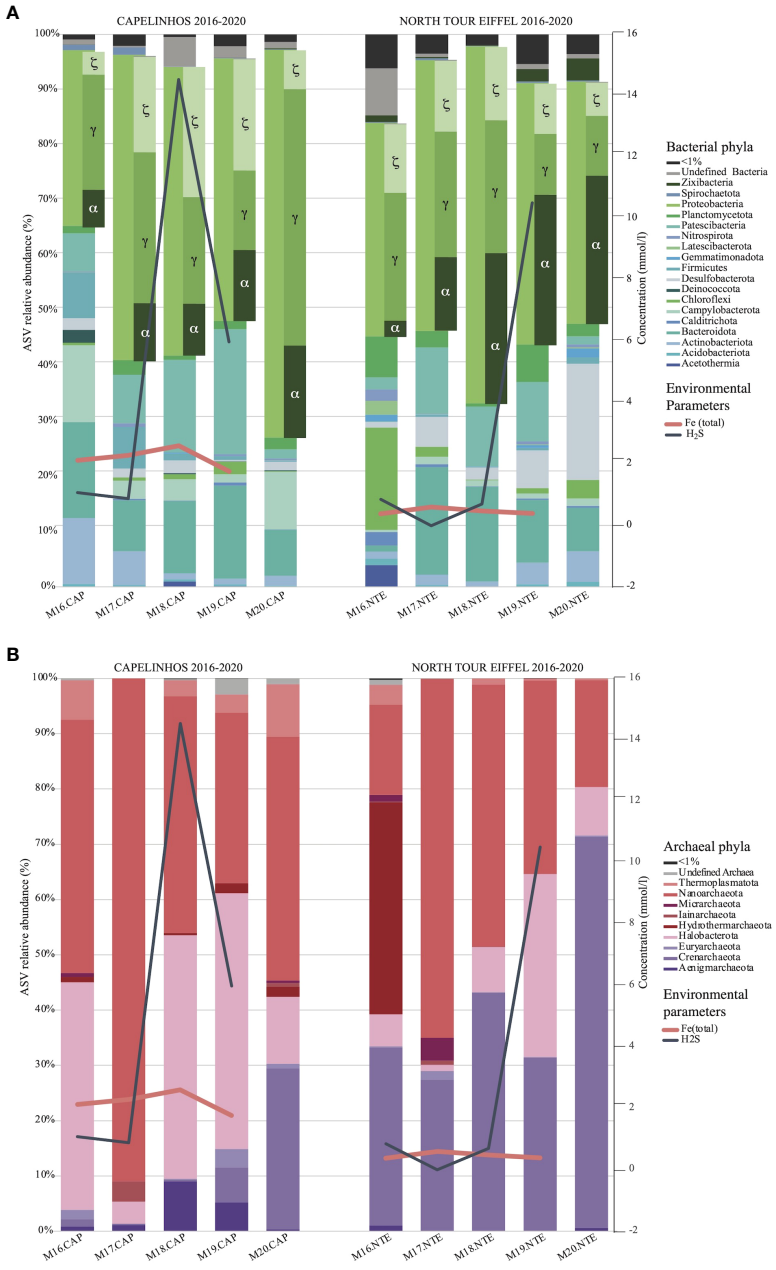

FIGURE 6
Bar plot depicting the abundance (%) of bacterial **(A)** and archaeal **(B)** phyla for each year (2016-2020) and for each site (Capelinhos in the left and North Tour Eiffel in the right). Only the phyla having an incidence higher than 1% are presented in the plot. The representation of the Proteobacteria phylum also includes the abundance of the different classes that conform it. Environmental parameters are represented as line plots superposed with the bar plots, depicting the concentration of dFe (pink) and dH_2S (grey) in each year and each site. Environmental parameters are not presented for 2020 as no hydrothermal fluid samples could be collected on that year due to the Covid-19 pandemic.

environment constrains their development and growth. Bacteroidota and Patescibacteria reproduced the same variations over time as Zetaproteobacteria at both sites. These two phyla could use the organic polymers excreted by Zetaproteobacteria to sustain their growth, which would explain why their abundance varies as that of Zetaproteobacteria (Xavier and Foster, 2007) and could corroborate their role as primary producers in the mats. Moreover, at Capelinhos we observed an inverse correlation between the variations of Zeta- and Gammaproteobacteria. This latter class was dominant in 2016, 2017 and 2020 (around 20.8 – 46.5%), and its incidence remained high in 2018 and 2019 (19.2% and 14.5%, respectively). At this site, Gammaproteobacteria was mostly represented by methane oxidizers. As previously mentioned, iron and methane oxidation has been observed to simultaneously occur in other iron-rich microbial mats (Quaiser et al., 2014). Our results suggest that there could exist a balancing mechanism between these two types of metabolisms, probably related to the variations of dFe concentration. This may suggest as well that these two types of microorganisms may act as primary producers inside the mats. At North Tour Eiffel, Gammaproteobacteria varied in accordance with Zetaproteobacteria (around 10.9 - 24%). Indeed, at this site this class was mostly represented by organotrophic bacteria.

Hydrothermalism vs current tidal-seawater influence on the temporal scale

The NMDS plots representing the beta diversity (Figure 7) allowed us to separate the samples into three main and distinctive clusters: 2016 samples, 2017-2019 samples, and 2020 samples. This was sustained by the db-RDA (Figure 4), which revealed that the 2018 and 2019 samples were more influenced by dH_2S concentration.

2016 - The structure of the microbial communities from both sites appeared different and more diversified than those of the other years. The alpha diversity index was higher in 2016 (Figure 2B), except for Archaea at Capelinhos, than in the following three years. At both sites, the bar plot (Figure 6) revealed a quite different microbial community composition, highlighting particularly the lowest abundance of Proteobacteria. At Capelinhos, this difference was evidenced through the abundance of Campylobacterota, which presented their highest incidence (13.9%) on that year. At North Tour Eiffel, this distinction was given by the lowest abundance of Alphaproteobacteria (2.9%), and the higher proportion of members of Chloroflexi and Hydrothermarchaeota (18.5% and 38.3%, respectively), compared to other years. Moreover, the archaeal community had the highest relative abundance (9.2%, Table S2 of the Supplementary Information) at this site on this year. All the phyla that presented higher abundances in 2016 were represented by microorganisms coming from hydrothermal environments, suggesting a higher proportion of end-member hydrothermal fluids in the diffuse fluids at both sites on that year. The continuous monitoring of geophysical processes occurring at LSHF allowed to identify either a volcanic/magmatic inflation event or a tectonic deformation taking place in September-October 2015 (Ballu et al., 2019). This event could have modified the physico-chemical composition of end-member hydrothermal fluids, as it has already been described in other hydrothermal environments (*e.g.* Lilley et al., 2003; Seewald et al., 2003). This could have affected the microbial communities developing there, explaining the higher diversity observed at both sites. Although we do not have a simultaneous sampling of both iron-rich microbial mats and black smoker hydrothermal fluids at the time of the event and knowing that microbial communities do not evolve on the same timescale as environmental parameters do, we could still observe the effect of this event in the microbial structures a few months later.

2017 to 2019 - While the beta diversity index (Figure 7) showed that the microbial communities remained quite similar during this period, we observed some variations on the alpha diversity (Figure 2B) and on the taxonomic composition (Figure 6). At Capelinhos, the bacterial communities were dominated by microorganisms coming from hydrothermal environments, but with an increasing contribution of seawater-born microorganisms. Overall, during these three years the structure of the bacterial communities showed a clear decrease of Campylobacterota (from 3.3% to 1.5%) and Gammaproteobacteria (from 27.4% to 14.5%), and an increase of Patescibacteria (from 8.8% to 22.6%) and Bacteroidota (from 9.3% to 16.9%). Alphaproteobacteria remained stable (10.5 - 12.8%), while Zetaproteobacteria showed small variations, achieving their maximal abundance in 2018 (23.7%), coinciding with the highest dFe concentration. Regarding the archaeal communities, they presented increasing relative abundances during these three years

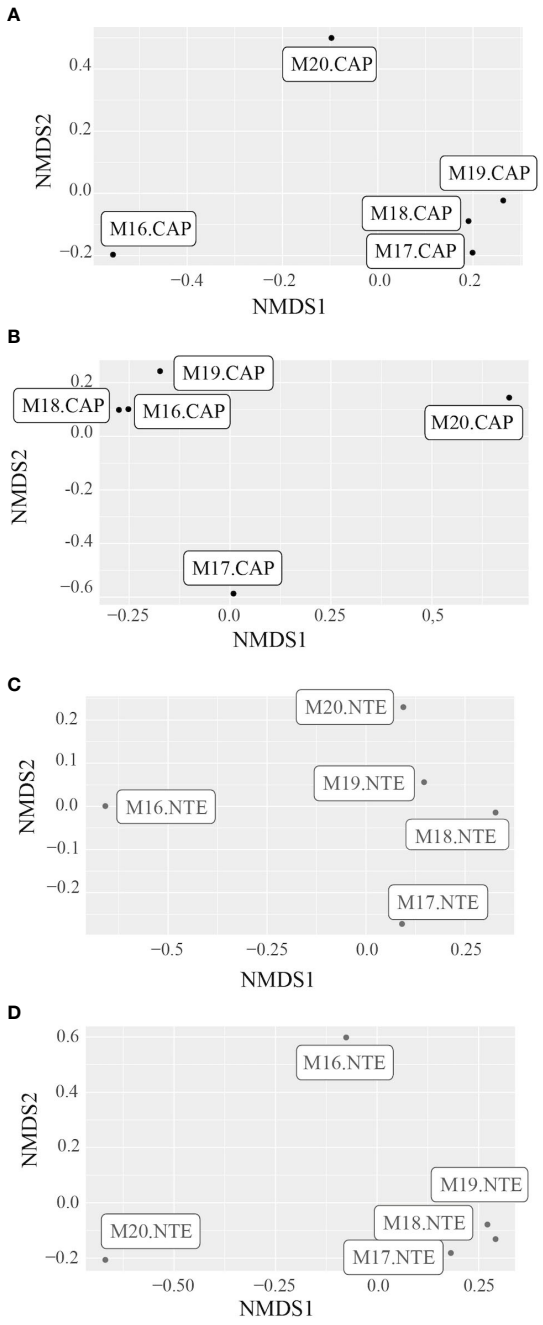

FIGURE 7
NMDS plot representing the differences between the bacterial communities' structure of the five samples from **(A)** Capelinhos (black) and **(C)** North Tour Eiffel (grey), and between the archaeal communities' structure of the five samples from **(B)** Capelinhos (black) and **(D)** North Tour Eiffel (grey).

(from a 0.5% of the total community in 2017 to an 8.6% in 2019, Table S2 of the Supplementary Information), as well as increasing alpha diversity indices (Figure 2B). Within them, we observed a strong decrease of Nanoarchaeota (from 91% to 30.9%), whose members are usually found in organic matter rich marine environments or are linked with symbiotic or parasitic lifestyles (Gründger et al., 2019), while Halobacterota, mostly represented by methane-oxidizing archaea (*Methanoperedenaceae* family), increased drastically from 2017 to 2018 (from 4% to 44%) and remained stable in 2019 (46.2%). Nonetheless, at the end of the 2017 - 2019

period, the increasing abundance of members of Patescibacteria, Bacteroidota, Alphaproteobacteria and Crenarchaeota (from 0.2% in 2017 and 2018 to 6.3% in 2019) (all mainly coming from seawater), could suggest an increasing influence of current tidal-related seawater on Capelinhos' mats. At North Tour Eiffel, between 2017 and 2019, both bacterial and archaeal communities experienced higher variations, as evidenced by the alpha diversity indices (Figure 2B). Zeta- and Gammaproteobacteria followed a decreasing trend (from 12.9% to 9.2% and from 22.8% to 10.9%, respectively), correlated with the decreasing dFe concentration in the end-member hydrothermal fluids. We observed an increasing abundance of Halobacterota (from 1.1% to 33.1%), mostly methanotrophic archaea, which could be due to an increasing contribution of end-member hydrothermal fluids in the diffuse fluids feeding the mats at this site. Over these three years, Alphaproteobacteria had an increasing tendency (from 13.2% to 27.2%). Within them, members of the *Roseobacter* clade were mostly represented. Moreover, Patescibacteria, Bacteroidota and Crenarchaeota remained quite abundant during this period (around 11%, 16% and 34%, respectively). As previously said, these are all seawater-related microorganisms. Overall, during this three years period at North Tour Eiffel, we observed an increasing influence of both the contribution of end-member hydrothermal fluids on the diffuse fluids, and of the current tidal-related seawater on the mats.

2020 – At both sites, we observed the highest incidences of Proteobacteria and Crenarchaeota (29.1% and 70.8%, for Crenarchaeota at Capelinhos and North Tour Eiffel, respectively). Indeed, Archaea presented very low relative abundances on this year (0.9% at Capelinhos and 2.4% at North Tour Eiffel, Table S2 of the Supplementary Information). Capelinhos presented the highest alpha diversity index for both the bacterial and the archaeal communities on this year (Figure 2B). The bacterial community was largely dominated by Gammaproteobacteria (46.5%), mostly related to methanotrophic and sulphur-oxidizing bacteria, with an increasing contribution of seawater-born microorganisms. The abundance of Campylobacterota, also sulphur-oxidizing bacteria, increased (10.5%) and Halobacterota had a lower abundance (12.1%). At North Tour Eiffel, even though the alpha diversity index for bacteria was lower than on the previous year (Figure 2B), a strong community variation was still evident, with a significant increase in Desulfobacterota (21%), linked to organotrophic and/or sulphate-reducing bacteria. The increasing abundance of organotrophic and seawater-born microorganisms on the microbial communities at both sites, indicated a higher seawater influence on the structuration of the iron-rich mats than on previous years.

Regional LSHF influence at the temporal scale

In 2016, the microbial communities of both sites had a higher occurrence of hydrothermal related microorganisms, potentially related to the geophysical event that took place some months before in 2015. Inversely, in 2020, both communities had a higher abundance of seawater related microorganisms, which could indicate that a regional LSHF hydrothermal circulation process may have occurred, shaping the communities at both sites independently of the environmental conditions and features of each site. Through EMSO-Azores seafloor observatory, we know that the hydrothermal circulation at this site is subject to variations at various timescales from days to years (Barreyre et al., 2014), impacting microbial communities (Rommevaux et al., 2019). Here we show that variations in the composition and contribution of end-member hydrothermal fluids in the diffuse fluids feeding the mats, shape and structure their microbial communities. Through these analyses, similar microbial community variations on both sites were observed over the 2016-to-2020 time interval. These changes in microbial community composition at the two studied sites indicate that there exists a regional LSHF influence at the temporal scale, probably related to variations in the contribution of end-member hydrothermal fluids to the diffuse fluids, in the composition of the end-member hydrothermal fluids themselves, and in the influence of current tidal-seawater above the mats.

Conclusion

Within this study we show that at LSHF, the composition and contribution of end-member hydrothermal fluids on the diffuse fluids nourishing iron-rich microbial mats have a strong influence on the structure of their microbial communities. Capelinhos and North Tour Eiffel end-member hydrothermal fluids differ from one another in terms of dFe concentration, *i.e.* the former being 4 - 7 times more enriched than the latter. As a result, the microbial community structures between Capelinhos and North Tour Eiffel sites are very distinctive, as evidenced by a dominance of microorganisms with metabolisms related to iron, methane, and reduced sulphur compounds at Capelinhos and a higher abundance of microorganisms with metabolisms related to organic compounds, nitrogen, and oxidized sulphur compounds at North Tour Eiffel. Therefore, the microbial community at Capelinhos seems to be more influenced by the diffuse fluids nourishing the mats while that of North Tour Eiffel seems to be more influenced by the seawater surrounding them.

We highlight the importance of iron-oxidizing and methanotrophic bacteria, both autotrophic, within these mats, being stronger at Capelinhos than at North Tour Eiffel. Moreover, we emphasize the co-existence between Zetaproteobacteria and *Nitrosopumilus*, which could indicate a link between iron and nitrogen cycles.

Finally, we present for the first time the variations in the community structure of these mats at each site as a function of environmental variations over time, thanks to EMSO-Azores seafloor observatory, allowing annual sampling campaigns. Through the present study, we highlight that a geological event took place in 2015 affecting 2016 communities' structures, and that a regional event could have occurred in 2020, as evidenced by a more diversified and completely different composition of the microbial communities on these years. We argue that there exists a regional LSHF effect at the temporal scale which affects the communities at both sites in the same way. Except for the years when a geological event took place, our study shows that the communities of iron-rich microbial mats remain stable over time at both sites.

Data availability statement

The original contributions presented in the study are publicly available. This data can be found here: NCBI, PRJNA798257 and the accession number for the BioSamples are SAMN25059546 - SAMN25059555.

Author contributions

AA-C planned and performed the microbiological experiments, performed the bioinformatic analyses and wrote the manuscript. MG planned and performed the microbiological experiments. AD helped to shape the presented idea and participated in the writing of the manuscript. VC conducted geochemical sampling, planned and performed the geochemical experiments and wrote the manuscript. CR conceived the presented idea, conducted the microbiological sampling, conceived, planned and performed the microbiological experiments, wrote the manuscript and supervised the project. All authors contributed to the article and approved the submitted version.

Funding

This project was funded by the French Oceanographic Fleet through the 2015 to 2020 cruises within the MoMAR program (France). This work was supported by a French National Research Agency (ANR) grant as part of the IRONWOMAN project (ANR-21-CE02-0012) and by the TelluS Post-Campagne grant (2016 – 2021) from CNRS-INSU. AA-C was supported by MESR PhD scholarship and Aix-Marseille University (MIO, France). The project leading to this publication has received funding from European FEDER Fund under project 1166-39417.

Acknowledgments

We would like to thank the heads of missions of the MoMAR 2015 to 2020 campaigns, as well as the sailors and underwater gear personnel of the French Oceanographic Fleet for samples collection. We thank captains, officers, and crew onboard R.V. *L'Atalante* and *PourquoiPas?* who made the series of Lucky Strike cruises possible. We thank the ROV *Victor* and HOV *Nautile* team for supporting our deep submergence field campaigns. We thank the scientific team, particularly the cruises PIs P.M. Sarradin and M. Cannat. We thank T. Audemar and C. Nicol for their contribution to molecular biology experiments during their internships.

Conflict of interest

The authors declare that the research was conducted in the absence of any commercial or financial relationships that could be construed as a potential conflict of interest.

Publisher's note

All claims expressed in this article are solely those of the authors and do not necessarily represent those of their affiliated organizations, or those of the publisher, the editors and the reviewers. Any product that may be evaluated in this article, or claim that may be made by its manufacturer, is not guaranteed or endorsed by the publisher.

Supplementary material

The Supplementary Material for this article can be found online at: https://www.frontiersin.org/articles/10.3389/fmars.2023.1038192/full#supplementary-material

References

Alain, K., Callac, N., Ciobanu, M.-C., Reynaud, Y., Duthoit, F., and Jebbar, M. (2011). DNA Extractions from deep subseafloor sediments: Novel cryogenic-mill-based procedure and comparison to existing protocols. *J. Microbiol. Methods* 87, 355–362. doi: 10.1016/j.mimet.2011.09.015

Allen, T. D., Lawson, P. A., Collins, M. D., Falsen, E., and Tanner, R. S. (2006). Cloacibacterium normanense gen. nov., sp. nov., a novel bacterium in the family flavobacteriaceae isolated from municipal wastewater. *Int. J. Syst. Evol. Microbiol.* 56, 1311–1316. doi: 10.1099/ijs.0.64218-0

Altschul, S. F., Gish, W., Miller, W., Myers, E. W., and Lipman, D. J. (1990). Basic local alignment search tool. *J. Mol. Biol.* 215, 403–410. doi: 10.1016/S0022-2836(05)80360-2

Ballu, V., Barreyre, T., Cannat, M., Testut, L., Crawford, W., Escartín, J., et al. (2019). What happened in 2015 at the lucky strike volcano? in. *Geophysical Res. Abstracts* 21, EGU2019–13294. EGU General Assembly 201. https://meetingorganizer.copernicus.org/EGU2019/EGU2019-13294.pdf.

Barreyre, T., Escartín, J., Garcia, R., Cannat, M., Mittelstaedt, E., and Prados, R. (2012). Structure, temporal evolution, and heat flux estimates from the lucky strike deep-sea hydrothermal field derived from seafloor image mosaics. *Geochemistry Geophys. Geosystems* 13, 1–29. doi: 10.1029/2011GC003990

Barreyre, T., Escartín, J., Sohn, R. A., Cannat, M., Ballu, V., and Crawford, W. C. (2014). Temporal variability and tidal modulation of hydrothermal exit-fluid temperatures at the lucky strike deep-sea vent field, mid-Atlantic ridge. *J. Geophys. Res. Solid Earth* 119, 2543–2566. doi: 10.1002/2013JB010478

Bauer, S., le, M., Roalkvam, I., Steen, I. H., and Dahle, H. (2016). Lutibacter profundi sp. nov., isolated from a deep-sea hydrothermal system on the arctic mid-ocean ridge and emended description of the genus lutibacter. *Int. J. Syst. Evol. Microbiol.* 66, 2671–2677. doi: 10.1099/ijsem.0.001105

Bayer, B., Vojvoda, J., Reinthaler, T., Reyes, C., Pinto, M., and Herndl, G. J. (2019). Nitrosopumilus adriaticus sp. nov. and nitrosopumilus piranensis sp. nov., two ammonia-oxidizing archaea from the adriatic sea and members of the class nitrososphaeria. *Int. J. Syst. Evol. Microbiol.* 69, 1892–1902. doi: 10.1099/ijsem.0.003360

Bennett, S. A., Toner, B. M., Barco, R., and Edwards, K. J. (2014). Carbon adsorption onto fe oxyhydroxide stalks produced by a lithotrophic iron-oxidizing bacteria. *Geobiology* 12, 146–156. doi: 10.1111/gbi.12074

Besson, P., Degboe, J., Berge, B., Chavagnac, V., Fabre, S., and Berger, G. (2014). Calcium, NA, K and Mg concentrations in seawater by inductively coupled plasma-atomic emission spectrometry: Applications to IAPSO seawater reference material, hydrothermal fluids and synthetic seawater solutions. *Geostand Geoanal Res.* 38, 355–362. doi: 10.1111/j.1751-908X.2013.00269.x

Cai, C., Leu, A. O., Xie, G. J., Guo, J., Feng, Y., Zhao, J. X., et al. (2018). A methanotrophic archaeon couples anaerobic oxidation of methane to Fe(III) reduction. *ISME J.* 12, 1929–1939. doi: 10.1038/s41396-018-0109-x

Callahan, B. J., McMurdie, P. J., Rosen, M. J., Han, A. W., Johnson, A. J. A., and Holmes, S. P. (2016). DADA2: High-resolution sample inference from illumina amplicon data. *Nat. Methods* 13, 581–583. doi: 10.1038/nmeth.3869

Cannat Mathilde (2018). *MOMARSAT2018 cruise, RV L'Atalante*. doi: 10.17600/18000514

Cannat, M., and Sarradin, P.-M. (2016). *MOMARSAT2016 cruise, RV L'Atalante*. doi: 10.17600/16001200

Castelle, C. J., Brown, C. T., Thomas, B. C., Williams, K. H., and Banfield, J. F. (2017). Unusual respiratory capacity and nitrogen metabolism in a parcubacterium (OD1) of the candidate phyla radiation. *Sci. Rep.* 7, 1–12. doi: 10.1038/srep40101

Chan, C. S., Fakra, S. C., Emerson, D., Fleming, E. J., and Edwards, K. J. (2011). Lithotrophic iron-oxidizing bacteria produce organic stalks to control mineral growth: Implications for biosignature formation. *ISME J.* 5, 717–727. doi: 10.1038/ismej.2010.173

Chan, C. S., McAllister, S. M., Leavitt, A. H., Glazer, B. T., Krepski, S. T., and Emerson, D. (2016). The architecture of iron microbial mats reflects the adaptation of chemolithotrophic iron oxidation in freshwater and marine environments. *Front. Microbiol.* 7. doi: 10.3389/fmicb.2016.00796

Charlou, J. L., Donval, J. P., Douville, E., Jean-Baptiste, P., Radford-Knoery, J., Fouquet, Y., et al. (2000). Compared geochemical signatures and the evolution of menez Gwen (37°50'N) and lucky strike (37°17'N) hydrothermal fluids, south of the Azores triple junction on the mid-Atlantic ridge. *Chem. Geol.* 171, 49–75. doi: 10.1016/S0009-2541(00)00244-8

Chavagnac, V., Leleu, T., Fontaine, F., Cannat, M., Ceuleneer, G., and Castillo, A. (2018). Spatial variations in vent chemistry at the lucky strike hydrothermal field, mid-Atlantic ridge (37°N): Updates for subseafloor flow geometry from the newly discovered capelinhos vent. *Geochemistry Geophys. Geosystems* 19, 4444–4458. doi: 10.1029/2018GC007765

Colaco, A., Blandin, J., Cannat, M., Carval, T., Connelly, D., et al. (2011). MoMAR-d: a technological challenge to monitor the dynamics of the lucky strike vent ecosystem. *ICES J. Mar. Sci.* 68 (2), 416–424. doi: 10.1093/icesjms/fsq075

Crépeau, V., Cambon Bonavita, M. A., Lesongeur, F., Randrianalivelo, H., Sarradin, P. M., Sarrazin, J., et al. (2011). Diversity and function in microbial mats from the lucky strike hydrothermal vent field. *FEMS Microbiol. Ecol.* 76, 524–540. doi: 10.1111/j.1574-6941.2011.01070.x

Cuvelier, D., Sarradin, P. M., Sarrazin, J., Colaço, A., Copley, J. T., Desbruyères, D., et al. (2011). Hydrothermal faunal assemblages and habitat characterisation at the Eiffel tower edifice (Lucky strike, mid-Atlantic ridge). *Mar. Ecol.* 32, 243–255. doi: 10.1111/j.1439-0485.2010.00431.x

Cuvelier, D., Sarrazin, J., Colaço, A., Copley, J., Desbruyères, D., Glover, A. G., et al. (2009). Distribution and spatial variation of hydrothermal faunal assemblages at lucky strike (Mid-Atlantic ridge) revealed by high-resolution video image analysis. *Deep Res. Part I Oceanogr Res. Pap* 56 (11), 2026–2040. doi: 10.1016/j.dsr.2009.06.006

Dahle, H., Økland, I., Thorseth, I. H., Pederesen, R. B., and Steen, I. H. (2015). Energy landscapes shape microbial communities in hydrothermal systems on the Arctic mid-ocean ridge. *ISME J.* 9, 1593–1606. doi: 10.1038/ismej.2014.247

Ding, W., Liu, P., Xu, Y., Fang, J., and Cao, J. (2019). Polyphasic taxonomic analysis of parasedimentitalea marina gen. nov., sp. nov., a psychrotolerant bacterium isolated from deep sea water of the new britain trench. *FEMS Microbiol. Lett.* 366 (22), fnaa004. doi: 10.1093/femsle/fnaa004

Einen, J., Thorseth, I. H., and Øvreås, L. (2008). Enumeration of archaea and bacteria in seafloor basalt using real-time quantitative PCR and fluorescence microscopy. *FEMS Microbiol. Lett.* 282, 182–187. doi: 10.1111/j.1574-6968.2008.01119.x

Emerson, D., and Moyer, C. L. (2002). Neutrophilic fe-oxidizing bacteria are abundant at the loihi seamount hydrothermal vents and play a major role in fe oxide deposition. *Appl. Environ. Microbiol.* 68, 3085–3093. doi: 10.1128/AEM.68.6.3085-3093.2002

Emerson, D., Rentz, J. A., Lilburn, T. G., Davis, R. E., Aldrich, H., Chan, C., et al. (2007). A novel lineage of proteobacteria involved in formation of marine fe-oxidizing microbial mat communities. *PloS One* 2 (8), e667. doi: 10.1371/journal.pone.0000667

Escartin, J., Barreyre, T., Cannat, M., Garcia, R., Gracias, N., Deschamps, A., et al. (2015). Hydrothermal activity along the slow-spreading lucky strike ridge segment (Mid-Atlantic ridge): Distribution, heatflux, and geological controls. *Earth Planet Sci. Lett.* 431, 173–185. doi: 10.1016/j.epsl.2015.09.025

Finster, K. W., Kjeldsen, K. U., Kube, M., Reinhardt, R., Mussmann, M., Amann, R., et al. (2013). Complete genome sequence of desulfocapsa sulfexigens, a marine deltaproteobacterium specialized in disproportionating inorganic sulfur compounds. *Stand Genomic Sci.* 8, 58–68. doi: 10.4056/sigs.3777412

Foster, Z. S. L., Sharpton, T. J., and Grünwald, N. J. (2017). Metacoder: An r package for visualization and manipulation of community taxonomic diversity data. *PloS Comput. Biol.* 13, 1–15. doi: 10.1371/journal.pcbi.1005404

Fouquet, Y., Charlou, J.-L., Costa, I., Donval, J.-P., Radford-Knoery, J., Pelle, H., et al. (1994). A detailed study of the lucky strike hydrothermal site discovery of a new hydrothermal site: Menez gwen; preliminary results of the DIVA1 cruise [5–29 may 1994]. *InterRidge News* 3, 14–17. https://archimer.ifremer.fr/doc/00070/18134/15682.pdf.

Gründger, F., Carrier, V., Svenning, M. M., Panieri, G., Vonnahme, T. R., Klasek, S., et al. (2019). Methane-fuelled biofilms predominantly composed of methanotrophic ANME-1 in Arctic gas hydrate-related sediments. *Sci. Rep.* 9, 1–10. doi: 10.1038/s41598-019-46209-5

Hager, K. W., Fullerton, H., Butterfield, D. A., and Moyer, C. L. (2017). Community structure of lithotrophically-driven hydrothermal microbial mats from the Mariana arc and back-arc. *Front. Microbiol.* 8. doi: 10.3389/fmicb.2017.01578

Haroon, M. F., Hu, S., Shi, Y., Imelfort, M., Keller, J., Hugenholtz, P., et al. (2013). Anaerobic oxidation of methane coupled to nitrate reduction in a novel archaeal lineage. *Nature* 500, 567–570. doi: 10.1038/nature12375

Hashimoto, Y., Tame, A., Sawayama, S., Miyazaki, J., Takai, K., and Nakagawa, S. (2021). Desulfomarina profundi gen. nov., sp. nov., a novel mesophilic, hydrogen-oxidizing, sulphate-reducing chemolithoautotroph isolated from a deep-sea hydrothermal vent chimney. *Int. J. Syst. Evol. Microbiol.* 71 (11). doi: 10.1099/ijsem.0.005083

Herlemann, D. P. R., Labrenz, M., Jürgens, K., Bertilsson, S., Waniek, J. J., and Andersson, A. F. (2011). Transitions in bacterial communities along the 2000 km salinity gradient of the Baltic Sea. *ISME J.* 5, 1571–1579. doi: 10.1038/ismej.2011.41

Holmes, D. E., Nicoll, J. S., Bond, D. R., and Lovley, D. R. (2004). Potential role of a novel psychrotolerant member of the family geobacteraceae, geopsychrobacter electrodiphilus gen. nov., sp. nov., in electricity production by a marine sediment fuel cell. *Appl. Environ. Microbiol.* 70, 6023–6030. doi: 10.1128/AEM.70.10.6023-6030.2004

Huber, H., Jannasch, H., Rachel, R., Fuchs, T., and Stetter, K. O. (1997). Archaeoglobus veneficus sp. nov., a novel facultative chemolithoautotrophic hyperthermophilic sulfite reducer, isolated from abyssal black smokers. *Syst. Appl. Microbiol.* 20, 374–380. doi: 10.1016/S0723-2020(97)80005-7

Iino, T., Mori, K., Uchino, Y., Nakagawa, T., Harayama, S., and Suzuki, K. I. (2010). Ignavibacterium album gen. nov., sp. nov., a moderately thermophilic anaerobic bacterium isolated from microbial mats at a terrestrial hot spring and proposal of ignavibacteria classis nov., for a novel lineage at the periphery of green sulfur bacteria. *Int. J. Syst. Evol. Microbiol.* 60 (Pt 6), 1376–1382. doi: 10.1099/ijs.0.012484-0

Jackson, C. R., Langner, H. W., Donahoe-Christiansen, J., Inskeep, W. P., and McDermott, T. R. (2001). Molecular analysis of microbial community structure in an arsenite-oxidizing acidic thermal spring. *Environ. Microbiol.* 3, 532–542. doi: 10.1046/j.1462-2920.2001.00221.x

Jeong, H. I., Jin, H. M., Jeon, C. O., et al. (2015). Confluentimicrobium naphthalenivorans sp. nov., a naphthalene-degrading bacterium isolated from sea-tidal-flat sediment, and emended description of the genus confluentimicrobium park. *Int. J. Syst. Evol. Microbiol.* 65 (11), 4191–4195. doi: 10.1099/ijsem.0.000561

Kallscheuer, N., Jogler, M., Wiegand, S., Peeters, S. H., Heuer, A., Boedeker, C., et al. (2020). Rubinisphaera italica sp. nov. isolated from a hydrothermal area in the tyrrhenian Sea close to the volcanic island panarea. *Antonie van Leeuwenhoek Int. J. Gen. Mol. Microbiol.* 113, 1727–1736. doi: 10.1007/s10482-019-01329-w

Kashefi, K., Tor, J. M., Holmes, D. E., Gaw Van Praagh, C. V., Reysenbach, A. L., and Lovley, D. R. (2002). Geoglobus ahangari gen. nov., sp. nov., a novel hyperthermophilic archaeon capable of oxidizing organic acids and growing autotrophically on hydrogen with Fe(III) serving as the sole electron acceptor. *Int. J. Syst. Evol. Microbiol.* 52, 719–728. doi: 10.1099/ijs.0.01953-0

Laufer, K., Nordhoff, M., Halama, M., Martinez, R. E., Obst, M., Nowak, M., et al. (2017). Microaerophilic Fe(II)-oxidizing zetaproteobacteria isolated from low-fe marine coastal sediments: Physiology and composition of their twisted stalks. *Appl. Environ. Microbiol.* 83, 1–20. doi: 10.1128/AEM.03118-16

Leleu, T. (2018). *Variabilité spatio-temporelle de la composition des fluides hydrothermaux (observatoire fond de mer EMSO-açores , lucky strike) : traçage de la circulation hydrothermale et quantification des flux chimiques associés to cite this version : HAL Id : tel-0*. https://archimer.ifremer.fr/doc/00692/80380/83501.pdf.

Leu, A. O., Cai, C., McIlroy, S. J., Southam, G., Orphan, V. J., Yuan, Z., et al. (2020). Anaerobic methane oxidation coupled to manganese reduction by members of the methanoperedenaceae. *ISME J.* 14, 1030–1041. doi: 10.1038/s41396-020-0590-x

Lilley, M. O., Butterfield, D. A., Lupton, J. E., and Olson, E. J. (2003). Magmatic events can produce rapid changes in hydrothermal vent chemistry. *Nature* 422, 878–881. doi: 10.1038/nature01569

Lim, J. K., Kim, Y. J., Yang, J. A., Namirimu, T., Yang, S. H., Park, M. J., et al. (2020). Thermococcus indicus sp. nov., a Fe(III)-reducing hyperthermophilic archaeon isolated from the onnuri vent field of the central Indian ocean ridge. *J. Microbiol.* 58, 260–267. doi: 10.1007/s12275-020-9424-9

Luo, H., and Moran, M. A. (2014). Evolutionary ecology of the marine roseobacter clade. *Microbiol. Mol. Biol. Rev.* 78, 573–587. doi: 10.1128/mmbr.00020-14

Makita, H. (2018). Iron-oxidizing bacteria in marine environments: recent progresses and future directions. *World J. Microbiol. Biotechnol.* 34, 0. doi: 10.1007/s11274-018-2491-y

Makita, H., Kikuchi, S., Mitsunobu, S., Takaki, Y., Yamanaka, T., Toki, T., et al. (2016). Comparative analysis of microbial communities in iron-dominated flocculent mats in deep-sea hydrothermal environments. *Appl. Environ. Microbiol.* 82, 5741–5755. doi: 10.1128/AEM.01151-16

McAllister, S. M., Moore, R. M., Gartman, A., Luther, G. W., Emerson, D., and Chan, C. S. (2019). The Fe(II)-oxidizing zetaproteobacteria: Historical, ecological and genomic perspectives. *FEMS Microbiol. Ecol.* 95, 1–18. doi: 10.1093/femsec/fiz015

McAllister, S. M., Vandzura, R., Keffer, J. L., Polson, S. W., and Chan, C. S. (2021). Aerobic and anaerobic iron oxidizers together drive denitrification and carbon cycling at marine iron-rich hydrothermal vents. *ISME J.* 15, 1271–1286. doi: 10.1038/s41396-020-00849-y

McMurdie, P. J., and Holmes, S. (2013). Phyloseq: An r package for reproducible interactive analysis and graphics of microbiome census data. *PloS One* 8 (4), e61217. doi: 10.1371/journal.pone.0061217

Mori, K., Suzuki, K. I., Yamaguchi, K., Urabe, T., and Hanada, S. (2015). Thiogranum longum gen. nov., sp. nov., an obligately chemolithoautotrophic, sulfur-oxidizing bacterium of the family ectothiorhodospiraceaeisolated from a deep-sea hydrothermal field, and an emended description of the genus thiohalomonas. *Int. J. Syst. Evol. Microbiol.* 65, 235–241. doi: 10.1099/ijs.0.070599-0

Moyer, C. L., Dobbs, F. C., and Karl, D. M. (1995). Phylogenetic diversity of the bacterial community from a microbial mat at an active, hydrothermal vent system, loihi seamount, Hawaii. *Appl. Environ. Microbiol.* 61, 1555–1562. doi: 10.1128/aem.61.4.1555-1562.1995

Muyzer, G., de Waal, E. C., and Uitterlinden, A. G. (1993). Profiling of complex microbial populations by denaturing gradient gel electrophoresis analysis of polymerase chain reaction-amplified genes coding for 16S rRNA. *Appl. Environ. Microbiol.* 59, 695–700. doi: 10.1128/aem.59.3.695-700.1993

Nakagawa, T., Koji, M., Hosoyama, A., Yamazoe, A., Tsuchiya, Y., Ueda, S., et al. (2021). Nitrosopumilus zosterae sp. nov., an autotrophic ammonia-oxidizing archaeon of phylum thaumarchaeota isolated from coastal eelgrass sediments of Japan. *Int. J. Syst. Evol. Microbiol.* 71 (8). doi: 10.1099/ijsem.0.004961

Oksanen, J, Simpson, G, Blanchet, F, Kindt, R, Legendre, P, Minchin, P, et al. (2020). *vegan: Community Ecology Package*. R package version 2.6-4. https://CRAN.R-project.org/package=vegan.

Ondréas, H., Cannat, M., Fouquet, Y., Normand, A., Sarradin, P. M., and Sarrazin, J. (2009). Recent volcanic events and the distribution of hydrothermal venting at the lucky strike hydrothermal field, mid-Atlantic ridge. *Geochemistry Geophys. Geosystems* 10 (2), 1–18. doi: 10.1029/2008GC002171

Oren, A., and Garrity, G. M. (2021). Valid publication of the names of forty-two phyla of prokaryotes. *Int. J. Syst. Evol. Microbiol.* 71 (10). doi: 10.1099/ijsem.0.005056

Park, S. C., Baik, K. S., Kim, D., and Seong, C. N. (2009). Maritimimonas rapanae gen. nov., sp. nov., isolated from gut microflora of the veined rapa whelk, rapana venosa. *Int. J. Syst. Evol. Microbiol.* 59, 2824–2829. doi: 10.1099/ijs.0.010504-0

Qin, W., Heal, K. R., Ramdasi, R., Kobelt, J. N., Martens-Habbena, W., Bertagnolli, A. D., et al. (2017). Nitrosopumilus maritimus gen. nov., sp. nov., nitrosopumilus cobalaminigenes sp. nov., nitrosopumilus oxyclinae sp. nov., and nitrosopumilus ureiphilus sp. nov., four marine ammoniaoxidizing archaea of the phylum thaumarchaeo. *Int. J. Syst. Evol. Microbiol.* 67, 5067–5079. doi: 10.1099/ijsem.0.002416

Quaiser, A., Bodi, X., Dufresne, A., Naquin, D., Francez, A. J., Dheilly, A., et al. (2014). Unraveling the stratification of an iron-oxidizing microbial mat by metatranscriptomics. *PloS One* 9, 1–9. doi: 10.1371/journal.pone.0102561

Quast, C., Pruesse, E., Yilmaz, P., Gerken, J., Schweer, T., Yarza, P., et al. (2013). The SILVA ribosomal RNA gene database project: Improved data processing and web-based tools. *Nucleic Acids Res.* 41, 590–596. doi: 10.1093/nar/gks1219

R Core Team (R Foundation for Statistical Computing) (2020) *R: A language and environment for statistical computing*. Available at: https://www.r-project.org/.

Reysenbach, A. L., Liu, Y., Banta, A. B., Beveridge, T. J., Kirshtein, J. D., Schouten, S., et al. (2006). A ubiquitous thermoacidophilic archaeon from deep-sea hydrothermal vents. *Nature* 442, 444–447. doi: 10.1038/nature04921

Reysenbach, A. L., and Shock, E. (2002). Merging genomes with geochemistry in hydrothermal ecosystems. *Sci. (80-)* 296, 1077–1082. doi: 10.1126/science.1072483

Rommevaux, C., Henri, P., Degboe, J., Chavagnac, V., Lesongeur, F., Godfroy, A., et al. (2019). Prokaryote communities at active chimney and *In situ* colonization devices after a magmatic degassing event (37°N MAR, EMSO-Azores deep-Sea observatory). *Geochemistry Geophys. Geosystems* 20, 3065–3089. doi: 10.1029/2018GC008107

Sarradin Pierre-Marie, C. M. (2015). MOMARSAT2015 cruise, RV pourquoi pas? doi: 10.17600/15000200

Sarradin Pierre-Marie, C. M. (2017). MOMARSAT2017 cruise, RV pourquoi pas? doi: 10.17600/17000500

Sarradin Pierre-Marie, L. J. (2019). MOMARSAT2019 cruise, RV pourquoi pas? doi: 10.17600/18001110

Sarradin Pierre-Marie, L. J. (2020). MOMARSAT2020 cruise, RV pourquoi pas? doi: 10.17600/18000684

Sarradin, P. M., Waeles, M., Bernagout, S., Le Gall, C., Sarrazin, J., and Riso, R. (2009). Speciation of dissolved copper within an active hydrothermal edifice on the lucky strike vent field (MAR, 37°N). *Sci. Total Environ.* 407, 869–878. doi: 10.1016/j.scitotenv.2008.09.056

Sarrazin, J., Legendre, P., de Busserolles, F., Fabri, M. C., Guilini, K., Ivanenko, V. N., et al. (2015). Biodiversity patterns, environmental drivers and indicator species on a high-temperature hydrothermal edifice, mid-Atlantic ridge. *Deep Res. Part II Top. Stud. Oceanogr* 121, 177–192. doi: 10.1016/j.dsr2.2015.04.013

Satola, B., Wübbeler, J. H., and Steinbüchel, A. (2013). Metabolic characteristics of the species variovorax paradoxus. *Appl. Microbiol. Biotechnol.* 97, 541–560. doi: 10.1007/s00253-012-4585-z

Scott, J. J., Breier, J. A., Luther, G. W., and Emerson, D. (2015). Microbial iron mats at the mid-atlantic ridge and evidence that zetaproteobacteria may be restricted to iron-oxidizing marine systems. *PloS One* 10, 1–19. doi: 10.1371/journal.pone.0119284

Scott, J. J., Glazer, B. T., and Emerson, D. (2016). Bringing microbial diversity into focus: high-resolution analysis of iron mats from the lō'ihi seamount. *Environ. Microbiol.* 19, 301–316. doi: 10.1111/1462-2920.13607

Seewald, J., Cruse, A., and Saccocia, P. (2003). Aqueous volatiles in hydrothermal fluids from the main endeavour field, northern Juan de fuca ridge: temporal variability following earthquake activity. *Earth Planet Sci. Lett.* 216, 575–590. doi: 10.1016/S0012-821X(03)00543-0

Sieber, C. M. K., Paul, B. G., Castelle, C. J., Hu, P., Tringe, S. G., Valentine, D. L., et al. (2019). Unusual metabolism and hypervariation in the genome of a gracilibacterium (BD1-5) from an oil-degrading community. *MBio* 10, e02128–e02119. doi: 10.1128/mBio.02128-19

Stahl, D. A., and Amann, R. (1991). Development and application of nucleic acid probes in bacterial systematics. In E. Stackebrandt and M. Goodfellow Eds. *Nucleic Acid Tech Bact Syst*. (Chichester: John Wiley & Sons Ltd.), 205–248.

Staley, J. T. (2010). ""Cycloclasticus: A genus of marine polycyclic aromatic hydrocarbon degrading bacteria,"," in *Handbook of hydrocarbon and lipid microbiology*. Ed. K. N. Timmis (Berlin, Heidelberg: Springer Berlin Heidelberg), 1781–1786. doi: 10.1007/978-3-540-77587-4_128

Steinsbu, B. O., Thorseth, I. H., Nakagawa, S., Inagaki, F., Lever, M. A., Engelen, B., et al. (2010). Archaeoglobus sulfaticallidus sp. nov., a thermophilic and facultatively lithoautotrophic sulfate-reducer isolated from black rust exposed to hot ridge flank crustal fluids. *Int. J. Syst. Evol. Microbiol.* 60, 2745–2752. doi: 10.1099/ijs.0.016105-0

Swingley, W. D., Sadekar, S., Mastrian, S. D., Matthies, H. J., Hao, J., Ramos, H., et al. (2007). The complete genome sequence of roseobacter denitrificans reveals a mixotrophic rather than photosynthetic metabolism. *J. Bacteriol.* 189 (3), 683–690. doi: 10.1128/JB.01390-06

Takai, K., and Horikoshi, K. (2000). Rapid detection and quantification of members of the archaeal community by quantitative PCR using fluorogenic probes. *Appl. Environ. Microbiol.* 66, 5066–5072. doi: 10.1128/AEM.66.11.5066-5072.2000

Tavormina, P. L., Hatzenpichler, R., McGlynn, S., Chadwick, G., Dawson, K. S., Connon, S. A., et al. (2015). Methyloprofundus sedimenti gen. nov., sp. nov., an obligate methanotroph from ocean sediment belonging to the 'deep sea-1' clade of marine methanotrophs. *Int. J. Syst. Evol. Microbiol.* 65, 251–259. doi: 10.1099/ijs.0.062927-0

Vander Roost, J., Thorseth, I. H., and Dahle, H. (2017). Microbial analysis of zetaproteobacteria and co-colonizers of iron mats in the troll wall vent field, Arctic mid-ocean ridge. *PloS One* 12, 1–18. doi: 10.1371/journal.pone.0185008

Von Damm, K. L. (1988). Systematics of and postulated controls on submarine hydrothermal solution chemistry. *J. Geophys. Res. Solid Earth* 93, 4551–4561. doi: 10.1029/JB093iB05p04551

Wang, S., Shao, Z., Lai, Q., Liu, X., Xie, S., Jiang, L., et al. (2021). Sulfurimonas sediminis sp. nov., a novel hydrogen- and sulfur-oxidizing chemolithoautotroph isolated from a hydrothermal vent at the longqi system, southwestern Indian ocean. *Antonie van Leeuwenhoek Int. J. Gen. Mol. Microbiol.* 114, 813–822. doi: 10.1007/s10482-021-01560-4

Wickham, H. (2016). *ggplot2: Elegant graphics for data analysistle* (New York: Springer-Verlag). Available at: https://ggplot2.tidyverse.org.

Xavier, J. B., and Foster, K. R. (2007). Cooperation and conflict in microbial biofilms. *Proc. Natl. Acad. Sci. U S A* 104, 876–881. doi: 10.1073/pnas.0607651104

Xu, L., Liu, A., and Zhang, Y. J. (2021). Zongyanglinia huanghaiensis gen. nov., sp. nov., a novel denitrifying bacterium isolated from the yellow sea, and transfer of pelagicola marinus to zongyanglinia gen. nov. as zongyanglinia marinus comb. nov. *Antonie van Leeuwenhoek Int. J. Gen. Mol. Microbiol.* 114, 137–149. doi: 10.1007/s10482-020-01507-1